Supporting Information

Bulk-Processed Pd Nanocube – Poly(methyl methacrylate) Nanocomposites as Plasmonic Plastic for Hydrogen Sensing

Iwan Darmadi[1, †], Alicja Stolaś[2, †], Ida Östergren[2, †], Barbara Berke[1], Ferry Anggoro Ardy Nugroho[1], Matteo Minelli[3], Sarah Lerch[2], Irem Tanyeli[1,4], Anja Lund[2], Olof Andersson[4], Vladimir P. Zhdanov[1,5], Marianne Liebi[1], Kasper Moth-Poulsen[2], Christian Müller[2]* and Christoph Langhammer[1]**

[1]Department of Physics, Chalmers University of Technology, 412 96 Göteborg, Sweden

[2]Department of Chemistry and Chemical Engineering, Chalmers University of Technology, 412 96 Göteborg, Sweden

[3]Department of Civil, Chemical, Environmental and Materials Engineering, University of Bologna, 40131 Bologna, Italy

[4]Insplorion AB, Medicinaregatan 8, 413 90 Göteborg, Sweden

[5]Boreskov Institute of Catalysis, Russian Academy of Sciences, Novosibirsk 630090, Russia

[†]equal contribution

* Correspondence to: kasper.moth-poulsen@chalmers.se, christian.muller@chalmers.se, clangham@chalmers.se

Table of Contents

1 Transmission Electron Microscopy of Pd Nanocubes After Synthesis and After Compounding

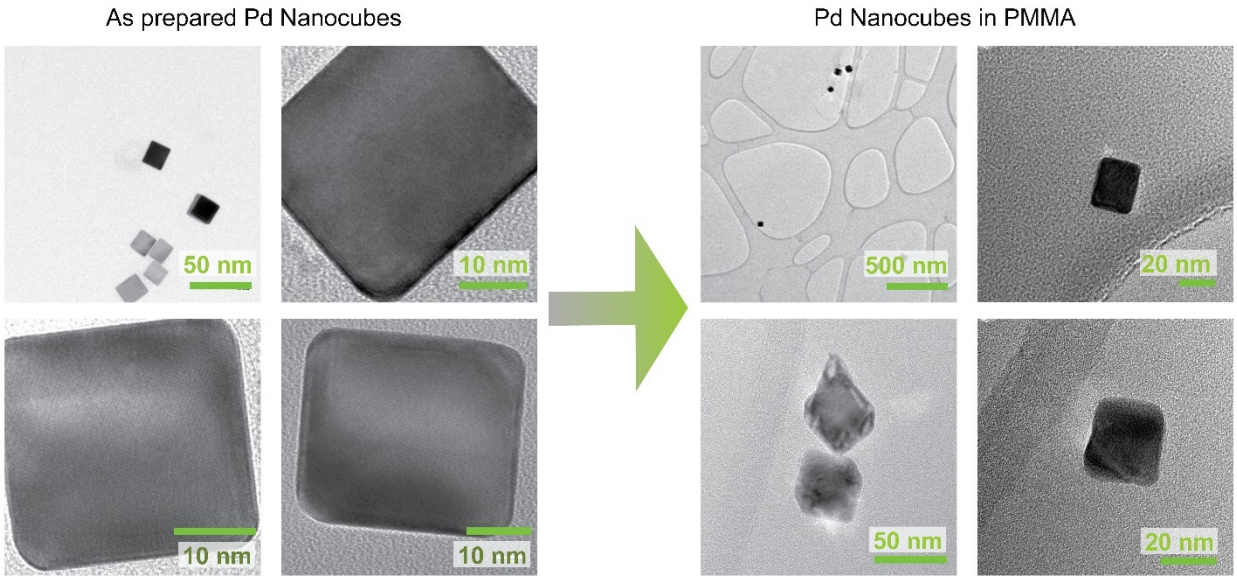

Figure SI 1. *High resolution TEM images of representative Pd nanocubes after synthesis and after compounding process.*

2 Small Angle X-Ray Scattering for Pd-Nanocube-PMMA

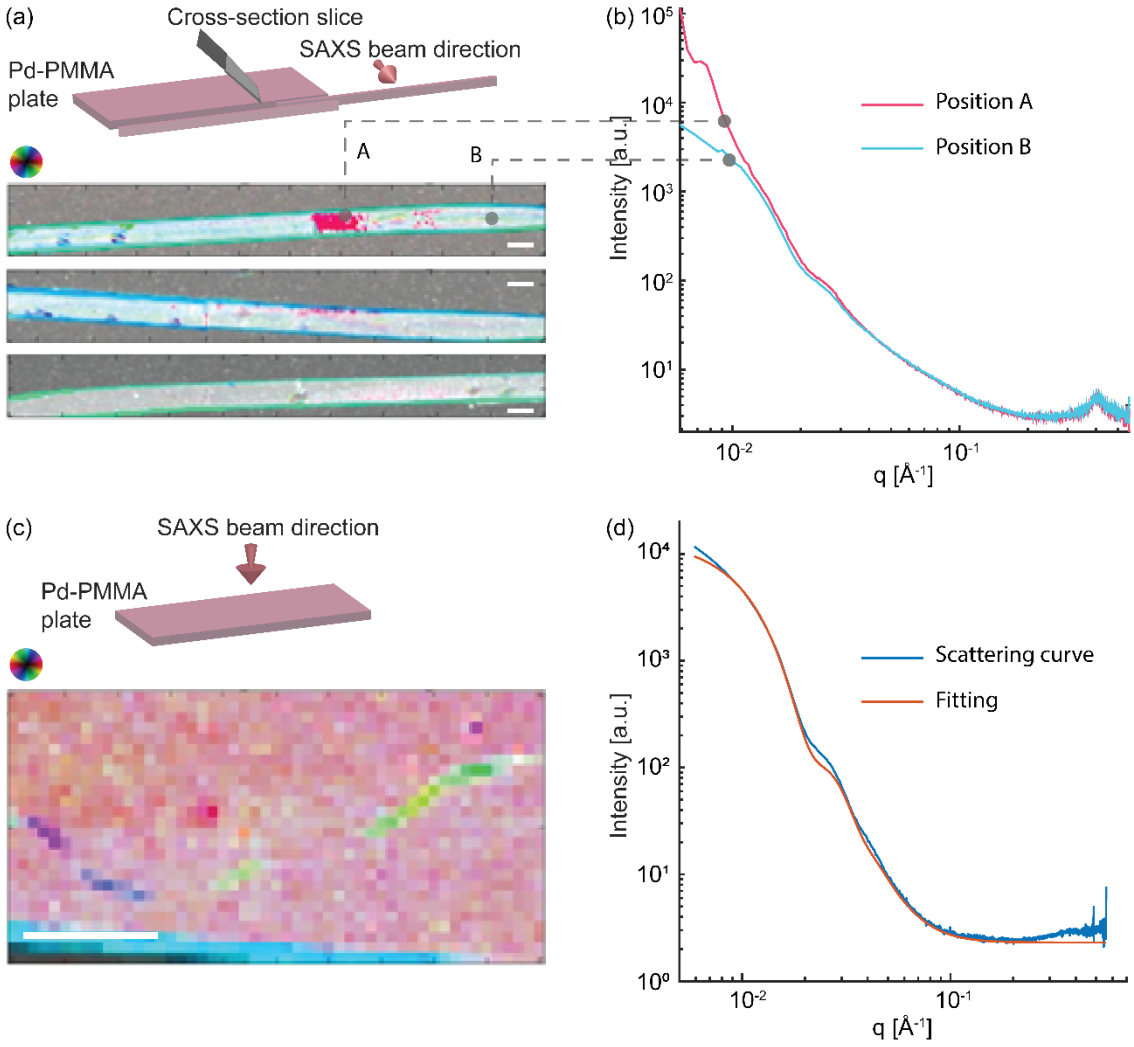

Figure SI 2. *(a) Scanning SAXS measurements of Pd-nanocube-PMMA plate cross-sections for 0.02 wt.% Pd concentration. The cross-section cut and the relative SAXS beam direction are illustrated. The cross-section thickness is 200 μm. The image combines the average scattering intensity, the oriented intensity and the preferred orientation angle (if there is any), according to the colour wheel, using a hue-saturation-value representation. A high density of oriented structures shows up as bright colours, whereas a high density of isotropically scattering structures will show up in white. Low scattering intensity would be represented by black areas. The white scale bars correspond to 500 μm. (b) Scattering signal of the two distinguishable regions in the sample cross section in (a). The upturn on the low Q region is attributed to the presence of nanoparticle aggregates. (c) Scanning SAXS measurement of a Pd-nanocube-PMMA lateral plane sample. The relative SAXS beam direction against the sample is illustrated. The sample thickness is 500 μm. The regions with different colours have the same scattering patterns, thus no aggregation is observed in this sample. (d) SAXS curve of Pd-nanocube-PMMA (blue curve) with the corresponding parallelepiped fit (red curve). The signal of neat PMMA has been subtracted. This data fitting is utilized to obtain the Pd nanocube size distribution summarized in* ***Table SI 1****.*

Table SI 1. *Average size (side-length) of Pd nanocubes in PMMA matrix obtained from SAXS fitting. The numbers are in good agreement with the dimensions obtained from TEM images from as-synthesized Pd nanocubes taken directly from the suspension after synthesis.*

Pd concentration (wt.%)	Sample thickness (μm)	Cut orientation	Average size of the cube (nm)
0.004	200	Cross section	25.4 ± 2.2
0.020	200	Cross section	27.1 ± 3.8
0.020	500	Lateral plane	29.7 ± 0.5
0.004	500	Lateral plane	29.7 ± 0.5
As-synthesized Pd-nanocubes, derived from TEM image analysis	-	-	23.2 ± 3.3

3 Pd Nanocubes Isotherm and Response/Recovery to/from 750 mbar Hydrogen Pressure

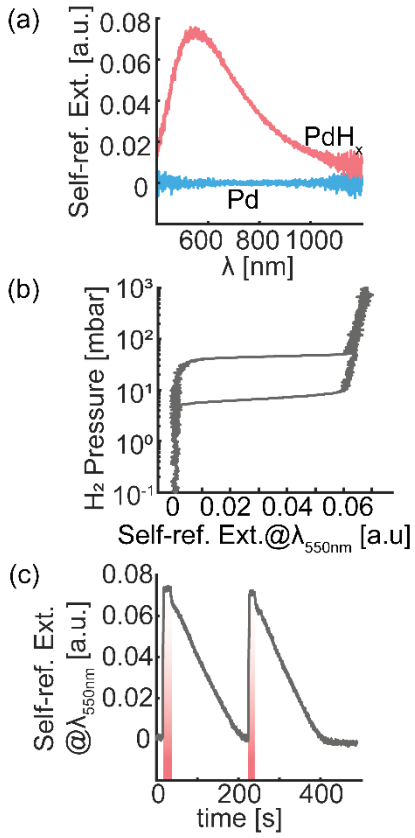

Figure SI 3. *(a) Self-referenced extinction spectra of Pd nanocubes drop-cast onto a glass substrate measured in vacuum (blue) and in 750 mbar H_2 gas (magenta). (b) Pressure vs self-referenced extinction@$\lambda_{550\ nm}$ isotherm measured at 30 ˚C for Pd nanocubes drop-cast onto a glass substrate. (c) Time evolution of the self-referenced extinction @$\lambda_{550\ nm}$ change in response to two pulses of 0 to 750 mbar H_2 (shaded areas). The average t_{50} for absorption and desorption were 1 and 72 s, respectively.*

4 Raw Data for Arrhenius Analysis of Hydrogen Sorption Kinetics

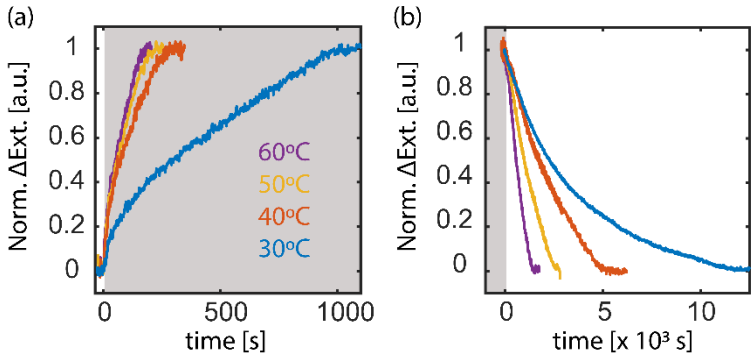

Figure SI 4. *Raw data used to construct the Arrhenius plot and calculate the apparent activation energies of hydrogen sorption for a Pd-nanocube-PMMA plate (0.03 wt.% loading and 500 µm thickness) displayed in* ***Figure 3d****. The kinetics measurements were performed at four different temperatures (30 ˚C, 40 ˚C, 50 ˚C, and 60 ˚C) by exposing the samples to a* H_2 *pressure step from 0 to 750 mbar for absorption, and to a step from 750 to 0 mbar for desorption. The grey-shaded areas in the figure indicate* H_2 *exposure.*

5 Calculation of Apparent Activation Energies of Hydrogen Sorption

The apparent activation energy for hydrogen sorption, E_a, is extracted from the Arrhenius plot using the Arrhenius equation:

$$k = Ae^{-\frac{E_a}{RT}} \tag{S1}$$

which is equivalent to:

$$ln\, k = ln\, A - \frac{E_a}{R}\left(\frac{1}{T}\right) \tag{S2}$$

where k is rate constant, A is the pre-exponential factor, R is the gas constant and T is absolute temperature (in K).

The rate (k) is assumed to be the inverse of the sorption time. For the sorption time, we use t_{50}, defined as the time needed to reach 50% of the maximum signal. Therefore, (S2) can be re-written as:

$$ln\frac{1}{t_{50}} = ln\, A - \frac{E_a}{R}\left(\frac{1}{T}\right) \tag{S3}$$

or

$$ln\, t_{50} = \frac{E_a}{R}\left(\frac{1}{T}\right) - ln\, A \tag{S4}$$

By plotting $ln\, t_{50}$ vs $\frac{1}{T}$ as in **Figure 3d** in the main text, E_a is obtained from the slope. The t_{50} is obtained from the kinetics data presented in **Figure SI 4**.

6 Raw Data for Derivation of Sorption Order Parameter

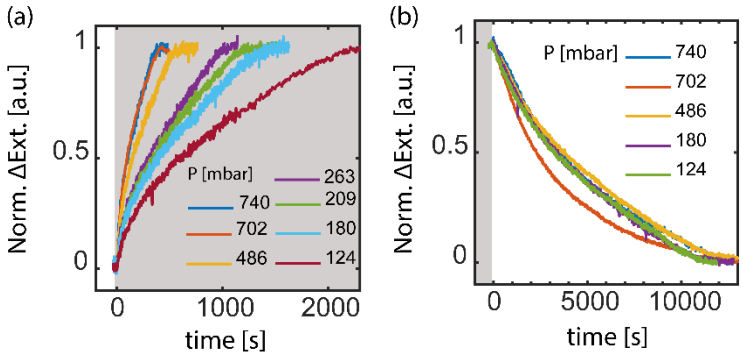

Figure SI 5. *Pressure-step dependent kinetics raw data used to construct and calculate the hydrogen ab- and desorption order parameters depicted in* ***Figure 3e*** *in the main text. The measurements were performed at 30˚C. The samples with thicknesses indicated by the legends were exposed to a H_2 pressure step from 0 to750 mbar for absorption, and to a step from 750 to 0 mbar for desorption. Grey-shaded areas indicate the H_2 gas exposure.*

7 Modelling of Hydrogen Sorption Kinetics of Pd-Nanocube-PMMA

7.1 Kinetic Model of Hydrogen sorption in Pd-Nanocube-PMMA Composite Plates

In the systems like the one under consideration here, the transient kinetics of hydrogen absorption and desorption depend on the ratios of some of the governing parameters. To specify these ratios, we first note that at equilibrium the H_2 concentrations in a Pd-nanocube-PMMA plate and in the gas phase are related as

$$c_f = \eta c_g \tag{S5}$$

where η is the partition coefficient. If the Pd nanoparticles are in the hydrogenated state, the corresponding effective H_2 concentration, c_{NP}, can be defined as one-half the concentration of H atoms calculated at the level of the plate, i.e.,

$$c_{NP} = 0.5\, c_0 C_{NP} V_{NP} \tag{S6}$$

where c_0 is the H concentration in the hydride, and C_{NP} and V_{NP} are the Pd nanoparticle concentration and volume. If $c_{NP} > c_f$, the potential capacity of nanoparticles with respect to hydrogen is higher than that of PMMA.

In addition, it is instructive to compare the scales of the rates of H_2 absorption (per unit volume) in two transient situations. The first one is when H_2 is absorbed by a neat PMMA plate in the absence of Pd nanoparticles. This process is controlled by H_2 diffusion in the plate, and the scale of its rate is given by the scale of the H_2 diffusion flux, $D\eta c_g/L$, divided by the plate thickness, L, i.e.

$$W_1 = \frac{D c_f}{L^2} = \frac{D\eta c_g}{L^2} \tag{S7}$$

where D is the H_2 diffusion coefficient. The opposite situation occurs when the H_2 diffusion is rapid, gradients of the H_2 concentration are negligible, and its value is given by (S5). In this case, the rate of H_2 absorption by the nanoparticles is given by

$$W_2 = k_a c_f C_{NP} = k_a \eta c_g c_{NP} \tag{S8}$$

where k_a is the absorption rate constant (it may depend on c_f and the extent of nanoparticle hydrogenation).

Physically, it is clear that if

$$c_f \gg c_{NP} \text{ or } \eta c_g \gg 0.5 c_0 c_{NP} V_{NP} \tag{S9}$$

the evolution of the H_2 concentration in the plate will be independent of nanoparticles, the average H uptake per nanoparticle will accordingly be independent of the nanoparticle concentration, and the response time will be independent of this concentration as well. In our experiments, the response time depends on the nanoparticle concentration. This means that condition (S9) does not hold in our case.

If condition (S9) doesn't hold, the situation depends on the ratio of rates in (S7) and (S8). In particular, the H_2 diffusion is fast compared to H_2 absorption by nanoparticles provided that

$$W_1 \gg W_2 \text{ or } \frac{D}{L^2} \gg k_a C_{NP}. \tag{S10}$$

In this case, gradients in the H_2 concentration are negligible, and its value is thus given by (S5), the average H uptake per nanoparticle is independent of the nanoparticle concentration, and the response time is independent on this concentration as well. In our experiments, as already mentioned, the response time depends on the nanoparticle concentration. This means that condition (S10) does not hold in case the response time is independent on nanoparticle concentration.

If conditions (S9) and (S10) are not fulfilled, gradients in the H_2 concentration in the composite plate during the transient hydrogenation period must be significant, and the transient kinetics of hydrogen absorption depend on the balance between H_2 diffusion in PMMA and absorption in the Pd nanoparticles dispersed in the PMMA. Analytically, this regime can be rationalized by using the approximation based on the concept of a *diffusion front*. In particular, we can introduce the front coordinate, l ($0 \leq l \leq L$). Behind the front, i.e. at $0 \leq x < l$, the H_2 concentration can be considered to drop from c_f to that, $\hat{c}_f^*$ ($\hat{c}_f^* \equiv \eta \hat{c}_g^*$), corresponding to the upper plateau of the absorption isotherm, and all the nanoparticles to be in the hydrogenated state. Ahead of the front, i.e. at $l \leq x < L$, the H_2 concentration can be considered to be below $\hat{c}_f^*$, and all the nanoparticles to be in the metallic state. The H_2 flux behind the front can be calculated in the steady-state approximation as $J = \frac{D\left(c_f - \hat{c}_f^*\right)}{l}$. This flux should be balanced by the hydrogenation of nanoparticles at the front, i.e., by $c_{NP}\left(\frac{dl}{dt}\right)$. Using this condition and expressing c_{NP} via C_{NP} (S6), we have

$$0.5 c_0 C_{NP} V_{NP} \frac{dl}{dt} = \frac{D\left(c_f - \hat{c}_f^*\right)}{l} \tag{S11}$$

The integration of this equation yields

$$l^2 = \frac{4\left(c_f - \hat{c}_f^*\right)Dt}{c_0 C_{NP} V_{NP}} \tag{S12}$$

The time scale of absorption or, in other words, the sensor response time can then be obtained by identifying l with L,

$$\tau_a = \frac{c_0 C_{NP} V_{NP} L^2}{4\left(c_f - \hat{c}_f^*\right)D} \tag{S13}$$

The dehydrogenation of the Pd nanoparticles can be analyzed in a similar way. Focusing again on the regime with significant gradients in H_2 concentration in the composite plate, we note that the process starts in the plate from a rapid diffusion-mediated drop of H_2 concentration down to that, $\check{c}_f^*$ ($\check{c}_f^* \equiv \eta \check{c}_g^*$), corresponding to the lower plateau of the desorption isotherm. During this phase, nanoparticles remain in the hydrogenated state. Then, there is a long dehydrogenation phase. To describe the latter phase, we again introduce the front coordinate, l ($0 \leq l \leq L$). Behind the front, i.e. at $0 \leq x < l$, the H_2 concentration can be considered to rise from zero at $x = 0$ (the H_2 concentration in the gas phase is assumed to be negligible) to $\check{c}_f^*$, and all the nanoparticles to be in the metal state. Ahead of the front, i.e. at $l \leq x < L$, the H_2 concentration can be considered to be equal to c_f^*, and all the nanoparticles to be in the

hydrogenated state. The H_2 flux behind the front can be represented as $J = D\check{c}_f^* / l$. This flux should be balanced by the dehydrogenation of nanoparticles at the front, i.e., by $c_{NP}(dl/dt)$, and accordingly we have

$$0.5 c_0 C_{NP} V_{NP} \frac{dl}{dt} = \frac{D\check{c}_f^*}{l}$$

or (S14)

$$l^2 = \frac{4Dt\check{c}_f^*}{c_0 C_{NP} V_{NP}}$$

The time scale of desorption or, in other words, the recovery time of the sensor can then be obtained by identifying l with L,

$$\tau_d = \frac{c_0 C_{NP} V_{NP} L^2}{4\check{c}_f^* D} \quad \text{(S15)}$$

7.2 Hydrogen Ab-/Desorption Kinetics for Different Pd Nanocube Concentrations

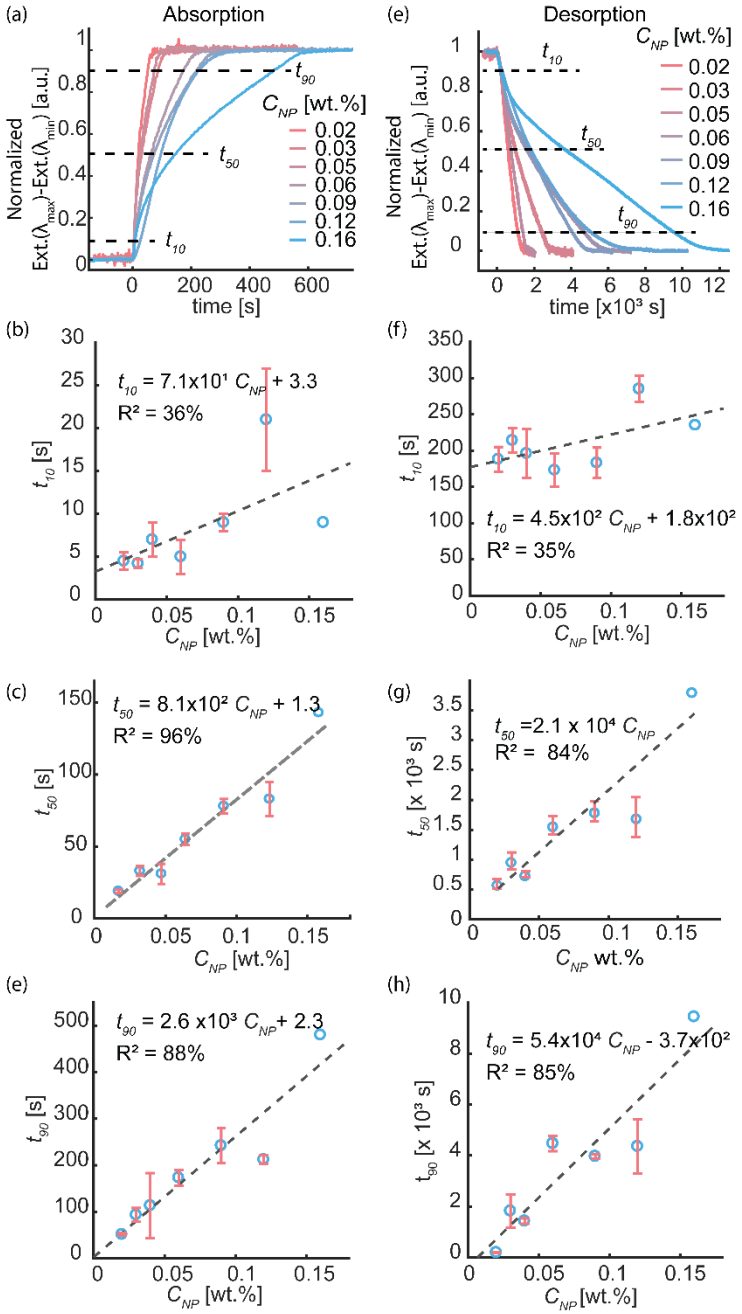

Figure SI 6 *Hydrogen absorption (a) and desorption (e) optical response of Pd-nanocube-PMMA composite plates with different Pd nanocube concentrations. The absorption response was recorded for a H_2 pressure step from 0 to 750 mbar, and the desorption response for a step from 750 to 0 mbar. The measurements were done at 30˚C. The correspondingly extracted t_{10}, t_{50}, and t_{90} parameters for absorption are presented in (b), (c) and (d), respectively. The t_{10}, t_{50}, and t_{90} for desorption response are shown in (f), (g) and (h), respectively. The dashed-lines denote fits to the kinetic model discussed above and are presented with the corresponding fitting values. Error bars depict the standard deviation from three measurements on each sample.*

The absorption and desorption optical response of Pd-nanocube-PMMA plates of 250 μm thickness with different Pd loading are presented in **Figure SI 6**. We used t_{10}, t_{50} and t_{90} to investigate the ab/desorption process at different stages along the reaction coordinate.

The early stage response for H_2 absorption, t_{10}, exhibits a weak linear trend with Pd nanoparticle concentration. The weak correlation indicates that two phenomena at the plate's surface may be dominating the process at the early stage of absorption: (i) the diluted H_2 concentration in the polymer matrix is larger than the hydrogen absorption capacity of the Pd nanoparticles and thus diffusion of H_2 in the polymer is not (completely) rate limiting (S9) or (ii) the hydrogen absorption rate into the Pd is significantly faster than H_2 diffusion in the PMMA (S10). At the later absorption stages, evidently, t_{50} and t_{90} exhibit a distinct linear correlation with Pd concentration. Hence, in agreement with our diffusion-front model (S13), the hydrogen absorption kinetics in the system is governed by a balance between hydrogen sorption and hydride formation in the Pd nanoparticles, and H_2 diffusion through the PMMA. Similarly, also for desorption, t_{50} and t_{90} correlate linearly with Pd nanoparticle concentration in the PMMA matrix, in good agreement with the diffusion-front model (S15).

7.3 Hydrogen Ab-/Desorption Kinetics for Composite Plates with Different Thickness

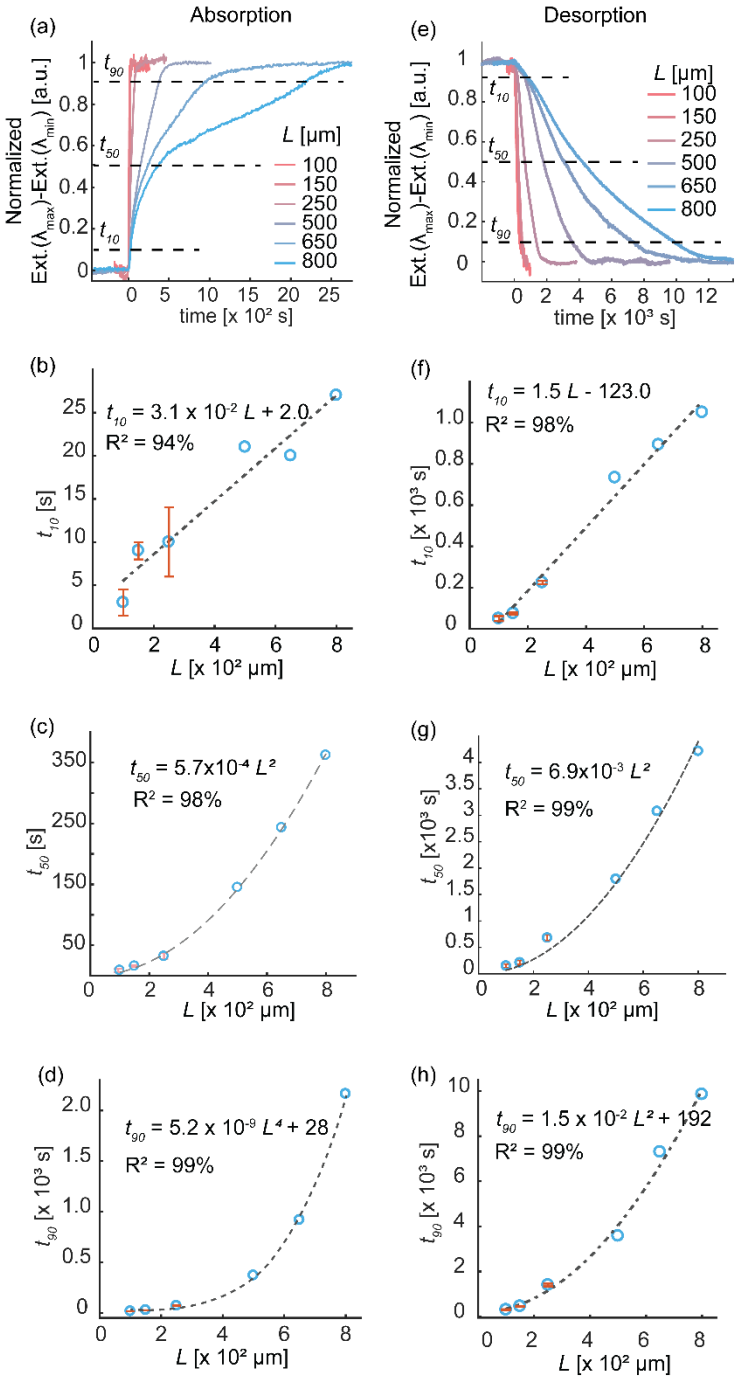

Figure SI 7. *Hydrogen absorption (a) and desorption (e) kinetics for Pd-nanocube-PMMA composite plates with thicknesses but constant Pd concentration. From the absorption kinetic curves in (a), t_{10}, t_{50}, and t_{90} are derived in (b), (c), and (d), respectively. For desorption, the corresponding t_{10}, t_{50}, and t_{90} are presented in (f), (g) and (h), respectively. The dashed-lines denote fits to the data. Error bars represent standard deviation from three measurements. The data without error bar were obtained from one measurement only.*

The absorption and desorption kinetic curves measured for Pd-nanocube-PMMA plates with thicknesses ranging from 100 – 800 μm upon exposure to a H_2 pressure step to/from 750 mbar are presented in **Figure SI 7**. To gain deeper mechanistic insight in the hydrogen absorption and desorption processes, we define three different time regimes and plot their descriptors t_{10}, t_{50} and t_{90} against the composite plate thickness. t_{10} then contains information about the early stages of the ab/desorption process at the plate surface, whereas t_{90} carries information about the ab/desorption process near saturation, and t_{50} corresponds to the half-way scenario.

Accordingly, t_{10} of the absorption process scales linearly with plate thickness, while t_{50} and t_{90} follows quadratic and quartic trends, respectively. To interpret these results, it is worth reminding ourselves that the gas absorption rate may either be limited by: (i) absorption processes at the plate surface or by (ii) gas diffusion from the plate surface into the plate bulk[1]. Accordingly, the thinner the plate, the more significant the surface effect and vice versa, when the plate is very thick, any surface effects may become negligible. From our data, it appears that during the initial phase of absorption (t_{10}) the rate limiting factor is plate surface absorption, indicated by the linear correlation with plate thickness (L) (**Figure SI 7b**). Specifically, in this early absorption stage, the hydrogen absorption into the Pd nanoparticles (which are in the solid solution α-phase and thus only consume little hydrogen) appears to be rate limiting, rather than gas diffusion through the PMMA matrix (see conditions (S9) and (S10)). On the other hand, t_{50} shows a quadratic trend with plate thickness (L), which then indicates that at this stage the rate limiting factor is the gas diffusion through the polymer[2] (**Figure SI 7c**). This is reasonable because at this stage, the Pd is undergoing the first order phase transformation to the hydride phase and thus consumes a lot of hydrogen, which cannot be supplied immediately by the polymer due to diffusion limitation. Hence, in this regime the diffusion-front model (S13) applies and we can derive the PMMA diffusivity (D) from our experimental data, as described below (**Subsection SI 8**).

Interestingly, t_{90} increases more dramatically with increasing plate thickness and exhibits a quartic dependence (**Figure SI 7d**). A possible explanation for this behavior in the late stages of hydrogenation is that, at the deeper level inside the composite, gas pressure drops dramatically because the Pd nanoparticles absorb large amounts of hydrogen. This explanation is supported by our direct H_2 gas transport measurements through 250 μm thick Pd-nanocube-PMMA composite plates, which show that the presence of Pd nanoparticles in the composite leads to a significantly longer time lag for H_2 to penetrate through the material compared to a neat PMMA plate (see **Section SI 8**). In this regime, the diffusion-front model does not describe the sorption process accurately anymore.

Now moving to discuss the desorption process, the t_{10} parameter for desorption (**Figure SI 7f**) follows similar linear trend as what we found for absorption but with a two orders of magnitude larger slope (**Figure SI 7b**). Specifically, if we compare the slopes for t_{10} desorption vs. t_{10} absorption, we find a ratio of 48. This ratio is of similar order than the ratio between desorption/absorption time we find for bare Pd nanocubes (72s/1s = 72, see **Figure SI 3c**). The similarity of these ratios and the fact that the trend is linear indicate that the rate-limiting factor in this regime is the Pd nanocube concentration via the hydrogen desorption process from the Pd into the matrix, and not the H_2 diffusivity in PMMA. This is again very reasonable since at this stage the nanoparticles are not yet decomposing the hydride phase (during which a lot of H_2 will be released) and thus only desorb small amounts.

The desorption t_{50} and t_{90} (**Figure SI 7g,h**) both follow quadratic trends, which implies that the rate limiting factor now is H_2 diffusion through the PMMA matrix, in agreement with our diffusion-front model (S15). For comparison, we note that in the diffusion-limited case [(S13)

and (S15)], the ratio of desorption and absorption time scales is expected to be $\frac{\tau_d}{\tau_a} = (c_f - \hat{c}_f^*)/\check{c}_f^*$. Taking relation (S5) into account, we can replace the concentrations in the plate by corresponding concentrations in the gas phase, i.e., $(c_g - \hat{c}_g^*)/\check{c}_g^*$. At our conditions with $c_g =$ 750 mbar, $\hat{c}_g^*$ = 40 mbar (pressure of PdH_x upper plateau), and $\check{c}_g^* = 6$ mbar (pressure of PdH_x lower plateau), we have $\frac{\tau_d}{\tau_a} = 118.3$. This ratio is larger than the actual ratio obtained by comparing the slope of absorption t_{50} vs desorption t_{50}: $\frac{t_{50}^d}{t_{50}^a} = 11.67$.

7.4 PMMA Diffusivity from Diffusion-Front Model for Pd Nanoparticle Concentration Variation in the Composite

For the interpretation of the experiment data, equation (S13) can be rewritten by analogy as equation (S16). In particular, L in equation (S13) is replaced by $\frac{L}{2}$ since the composite plate is exposed to H_2 from two sides. Furthermore, t_{50} is used to replace the time descriptor τ in equation (S13) and thereby introduces a factor 4 in the denominator, *i.e.*,

$$t_{50}^a = \frac{c_0 V_{NP} L^2 C_{NP}}{64\left(c_f - \hat{c}_f^*\right) D} \equiv k_a^{conc} C_{NP} \tag{S16}$$

where $k_a^{conc} = \frac{c_0 V_{NP} L^2}{64\left(c_f - c_f^*\right) D}$

The values of all variables:

- $k_a^{conc} = 8.1 \times 10^2 \frac{\text{s}}{\text{wt.\%}} = 1.0 \times 10^{-11} \frac{\text{s}}{\text{cm}^3}$ (obtained from the absorption t_{50} fitting in **Figure SI 6c**)
- $L = 250\ \mu\text{m} = 0.025$ cm
- $c_0 = 0.068 \frac{\text{mol}}{\text{cm}^3}$
- $V_{NP} = 1.2 \times 10^{-17}$ cm^3
- $C_{NP} = 1.25 \times 10^{12}$ cm^{-3}
- $P_m = 4.8$ barrer $= 1.6 \times 10^{-17} \frac{\text{mol}}{\text{cm Pa s}}$ (experimentally determined permeability of H_2 in PMMA, see **Section SI 8**)
- $\Delta\hat{p} = p_{ext} - p_{\,PdH_x\ upper\ plateau} = (7.5 \times 10^4 - 0.4 \times 10^4)\text{Pa} = 7.1 \times 10^4$ Pa (The PdH_x upper plateau pressure is defined from **Figure SI 3b**)

- $D_{exp} = 6.3 \times 10^{-7} \frac{\text{cm}^2}{\text{s}}$ (experimentally determined diffusivity of H_2 in PMMA, see **Section SI 8**)
- $c_f - \hat{c}_f^* = \frac{P_m \Delta \hat{p}}{D_{exp}} = 1.9 \times 10^{-6} \frac{\text{mol}}{\text{cm}^3}$

gives

$$D = \frac{c_0 V_{NP} L^2}{64\left(c_f - \hat{c}_f^*\right) k_a^{conc}} = \frac{0.068 \times 1.2 \times 10^{-17} \times (0.025)^2}{64 \times 1.9 \times 10^{-6} \times 1.0 \times 10^{-11}} = 4.4 \times 10^{-7} \frac{\text{cm}^2}{\text{s}}$$

And by rewriting equation (S15) as equation (S17) by analogy,

$$t_{50}^d = \frac{c_0 C_{NP} V_{NP} L^2}{64 \check{c}_f^* D} \equiv k_d^{conc} C_{NP} \tag{S17}$$

where

- $k_d^{conc} = 2.1 \times 10^4 \frac{\text{s}}{\text{wt.\%}} = 2.6 \times 10^{-10} \frac{\text{s}}{\text{cm}^3}$ obtained from the desorption t_{50} fitting (**Figure SI 6g**)
- $\Delta \check{p} = p_{\text{PdH}_x\ lower\ plateau} - p_{ext} = (0.06 \times 10^4 - 0)\text{Pa} = 6 \times 10^2$ Pa (The PdH_x lower plateau pressure is defined from **Figure SI 3b**)
- $\check{c}_f^* = \frac{P_m \Delta \check{p}}{D_{exp}} = 1.5 \times 10^{-8} \frac{\text{mol}}{\text{cm}^3}$

diffusivity is calculated from desorption data fitting,

$$D = \frac{c_0 V_{NP} L^2}{64 \check{c}_f^* k_d^{conc}} = \frac{0.068 \times 1.2 \times 10^{-17} \times (0.025)^2}{64 \times 1.5 \times 10^{-8} \times 2.6 \times 10^{-10}} = 2.1 \times 10^{-6} \frac{\text{cm}^2}{\text{s}}$$

7.5 PMMA Diffusivity from Diffusion-Front Model for Thickness Variation

Equation (S13) is rewritten by analogy as equation (S18),

$$t_{50}^a = \frac{c_0 C_{NP} V_{NP} L^2}{64\left(c_f - \hat{c}_f^*\right) D} \equiv k_a^{thick} L^2 \tag{S18}$$

where $k_a^{thick} = \frac{c_0 C_{NP} V_{NP}}{64\left(c_f - c_f^*\right)D}$

The values of all variables:

- $k_a^{thick} = 5.7 \times 10^4 \frac{\text{cm}^2}{\text{s}}$ obtained from the absorption t_{50} fitting **Figure SI 7c**.
- $c_0 = 0.068 \frac{\text{mol}}{\text{cm}^3}$
- $V_{NP} = 1.2 \times 10^{-17}\ \text{cm}^3$
- $C_{NP} = 1.25 \times 10^{12}\ \text{cm}^{-3}$
- $P_m = 4.8\ \text{barrer} = 1.6 \times 10^{-17} \frac{\text{mol}}{\text{cm Pa s}}$ (experimentally determined permeability of H_2 in PMMA, see **Section SI 8**)
- $\Delta\hat{p} = p_{ext} - p_{\ PdH_x\ upper\ plateau} = (7.5 \times 10^4 - 0.4 \times 10^4)\ \text{Pa} = 7.1 \times 10^4\ \text{Pa}$ (The PdH_x upper plateau pressure is defined from **Figure SI 3b**)
- $D_{exp} = 6.3 \times 10^{-7} \frac{\text{cm}^2}{\text{s}}$ (experimentally determined diffusivity of H_2 in PMMA, see **Section SI 8**)
- $c_f - \hat{c}_f^* = \frac{P_m \Delta\hat{p}}{D_{exp}} = 1.9 \times 10^{-6} \frac{\text{mol}}{\text{cm}^3}$

we have

$$D = \frac{c_0 C_{NP} V_{NP}}{64\left(c_f - \hat{c}_f^*\right)k_a^{thick}} = \frac{0.068 \times 1.25 \times 10^{12} \times 1.2 \times 10^{-17}}{64 \times 1.9 \times 10^{-6} \times 5.7 \times 10^4} = 1.6 \times 10^{-7} \frac{\text{cm}^2}{\text{s}}$$

Similar calculation from the desorption fitting,

$$t_{50}^d = \frac{c_0 C_{NP} V_{NP} L^2}{64 \check{c}_f^* D} \equiv k_d^{thick} L^2 \tag{S19}$$

where $k_d^{thick} = \frac{c_0 C_{NP} V_{NP}}{64 \check{c}_f^* D}$

with some values:

- $k_d^{thick} = 6.9 \times 10^5 \frac{\text{cm}^2}{\text{s}}$ from desorption t_{50} fitting **Figure SI 7g**
- $\Delta\check{p} = p_{PdH_x\ lower\ plateau} - p_{ext} = (0.06 \times 10^4 - 0)\ \text{Pa} = 6 \times 10^2\ \text{Pa}$ (The PdH_x lower plateau pressure is defined from **Figure SI 3b**)

- $\check{c}_f^* = \frac{P_m \Delta \check{p}}{D_{exp}} = 1.5 \times 10^{-8} \frac{\text{mol}}{\text{cm}^3}$

we obtain

$$D = \frac{c_0 C_{NP} V_{NP}}{64 \check{c}_f^* k_d^{thick}} = \frac{0.068 \times 1.25 \times 10^{12} \times 1.2 \times 10^{-17}}{64 \times 1.5 \times 10^{-8} \times 6.9 \times 10^5} = 1.5 \times 10^{-6} \frac{\text{cm}^2}{\text{s}}$$

Table SI 2. *Summary of the diffusivity calculations based on the diffusion front model.*

Diffusion-front model fitting	D [**cm²/s**]
Absorption t_{50} (concentration variation)	4.4×10^{-7}
Desorption t_{50} (concentration variation)	2.1×10^{-6}
Absorption t_{50} (thickness variation)	1.6×10^{-7}
Desorption t_{50} (thickness variation)	1.5×10^{-6}

8 Hydrogen Diffusion and Permeability Measurements on Neat PMMA and Pd-Nanocube-PMMA Plates

The H_2 transport properties were measured by direct permeation experiments using a manometric technique (ASTM Standard norm D 1434)[3]. The penetrant flux through the membrane was evaluated from the pressure increase in a calibrated closed volume, starting from high vacuum conditions. The tests were carried out in an apparatus described elsewhere[4]. It features a capacitive gauge (Edwards Barocell, 0-10 mbar range, sensitivity 0.001 mbar) to measure the gas pressure in the downstream compartment of the sample, while the upstream pressure was kept constant above atmospheric pressure, at approximately 1.2-1.5 bar (Druck, 0-10 bar). The whole experimental apparatus was enclosed in a thermostatic chamber (PID control, sensitivity 0.1 K).

The neat polymer and nanocomposite samples were first placed in the sample holder (Millipore, effective permeation area 2.2 cm^2) set across the two closed volumes and treated overnight under vacuum to remove all possible residual sorbed species. The diffusivity measurements were then carried out by connecting the high-pressure chamber with the specimen and terminated only after steady state conditions had been achieved, as observed as linear increase of downstream pressure over time. Each test was repeated at least twice to ensure the reproducibility of data obtained. The gas permeability, P, was then calculated as:

$$P = J_{ss}\frac{l}{\Delta p} = \left(\frac{dp_d}{t}\right)_{t\to+\infty}\frac{V_d}{R\,\mathrm{T}}\frac{l}{A\,\Delta p} \tag{S20}$$

where J_{ss} is the penetrant molar flux per unit area (at the steady state), Δp the pressure difference, p_d the downstream pressure, V_d the calibrated volume of the downstream side and A the membrane area.

Diffusion kinetics were evaluated by the time-lag method, which represents the process characteristic time. Its value, θ_L, was determined as the intercept on the time axis of the straight line, which describes the p_d vs. t curve at long times, i.e., at the steady state conditions. The diffusivity, D, can thus be calculated as[5]:

$$D = \frac{l^2}{6\theta_L} \tag{S21}$$

H_2 permeation tests were carried out at 35°C and He was used as reference for a non-reacting penetrant.

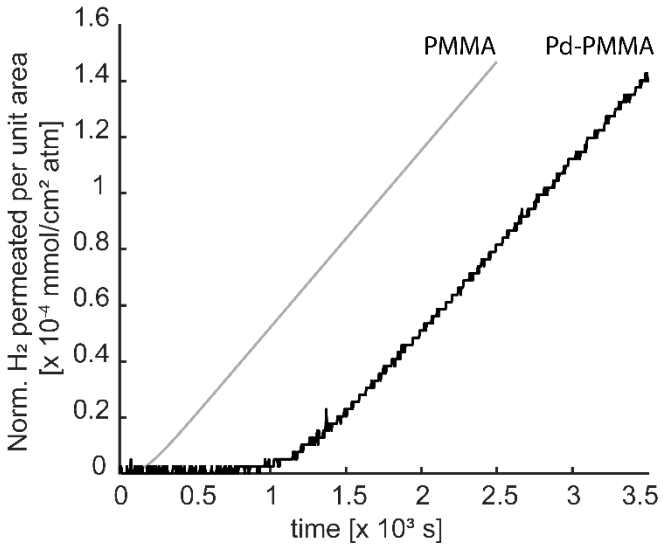

Figure SI 8. *H_2 permeability measurements for neat PMMA and Pd-nanocube-PMMA composite with 0.15 wt% Pd loading. The results are normalized with respect to the sample thickness.*

Table SI 3. *Data summary for H_2 and He lag time (t_L), permeability (P) and diffusivity (D) measurements on neat PMMA and Pd-nanocube-PMMA plates with 112 μm and 257 μm thickness.*

Sample	Thickness [μm]	Gas	TR [GPU]	θ_L [s]	P [Barrer]	D × 10^{-7} [cm^2/s]
PMMA	112	He	0.0871	7 ± 1	9.76 ± 0.02	29 ± 7
		H_2	0.0428	33 ± 1	4.79 ± 0.01	6.3 ± 0.4
	257*	H_2	0.0186	175	4.79	6.3
Pd-nanocube-PMMA (0.15 wt.% Pd)	257	He	0.0371	38 ± 10	9.54 ± 0.1	29 ± 9
		H_2	0.0185	1251	4.75 ± 0.04	0.9

*PMMA sample-data calculated for the 257 μm thickness.

For helium permeability and diffusivity of neat PMMA plates and Pd-nanocube-PMMA plates the same values are obtained, indicating that the presence of the Pd nanoparticles as such has no effect on the diffusion of a small and non-reacting penetrant.

For H_2 permeability of neat PMMA plates and Pd-nanocube-PMMA plates the same values are obtained, which means that in steady state the transport of H_2 through PMMA is not affected by the presence of Pd.

Interestingly, however, for H_2 diffusivity in neat PMMA plates and Pd-nanocube-PMMA plates, respectively, quite different values are obtained. This indicates that for Pd-nanocube-PMMA indeed an *apparent* diffusivity is obtained, which is a consequence of the hydride formation reaction that transiently captures and consumes H_2 molecules, thus preventing them from reaching the downstream side of the membrane.

9 Hydrogen Gas Sensing Test Setups

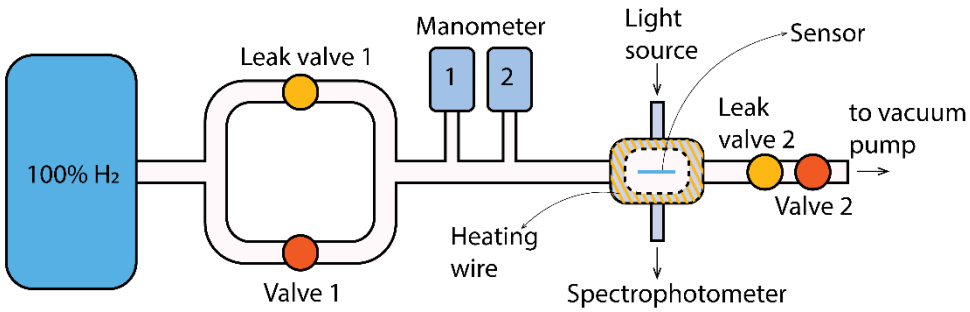

Figure SI 9. *Schematic depiction of the vacuum-chamber used for hydrogen optical pressure-composition isotherm and kinetics measurements.*

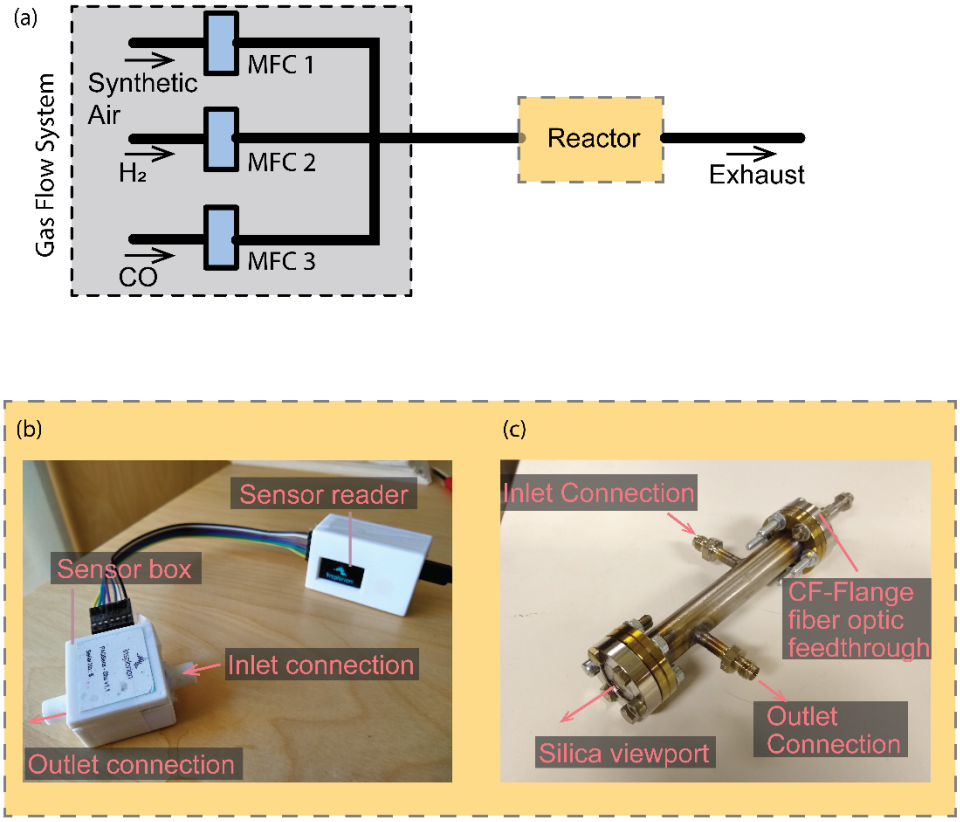

Figure SI 10. *(a) Schematic of the gas flow and humidifier setup used for H_2 sensing tests. The gas mixture and flow at atmospheric pressure is controlled by mass flow controllers (MFCs). (b) For the H_2 sensor demo with the InAir Hydec prototype, the reactor part was replaced by the sensor unit. (c) For the 3D printed sensor cap test, the reactor used is shown in. It is equipped with a CF-flange silica viewport and a CF-flange fibre optic feedthrough. The sensor cap was mounted onto the inner fibre tip of the feedthrough and the optical readout was recorded through the fused silica viewport.*

References

(1) Firpo, G.; Angeli, E.; Guida, P.; Pezzuoli, D.; Repetto, D.; Repetto, L.; Valbusa, U. The Role of Surfaces in Gas Transport through Polymer Membranes. *Polymers (Basel)*. **2019**, *11* (5), 910.

(2) Choudalakis, G.; Gotsis, A. D. Permeability of Polymer/Clay Nanocomposites: A Review. *Eur. Polym. J.* **2009**, *45* (4), 967–984.

(3) ASTM International. ASTM D1434-82: Standard Test Method for Determining Gas Permeability Characteristics of Plastic Film and Sheeting. *Annu. B. ASTM Stand.* **2009**, *82* (Reapproved 2015), 615.

(4) Minelli, M.; De Angelis, M. G.; Doghieri, F.; Marini, M.; Toselli, M.; Pilati, F. Oxygen Permeability of Novel Organic-Inorganic Coatings: I. Effects of Organic-Inorganic Ratio and Molecular Weight of the Organic Component. *Eur. Polym. J.* **2008**, *44* (8), 2581–2588.

(5) Crank, J. *The Mathematics of Diffusion*; Clarendon Press, 1975.